AIP Advances

Exchange coupling and microwave absorption in core/shell-structured hard/soft ferrite-based $CoFe_2O_4/NiFe_2O_4$ nanocapsules

Cite as: AIP Advances **7**, 056403 (2017); https://doi.org/10.1063/1.4972805
Submitted: 23 September 2016 . Accepted: 06 October 2016 . Published Online: 20 December 2016

Chao Feng, Xianguo Liu, Siu Wing Or, and S. L. Ho

Exchange coupling and microwave absorption in core/shell-structured hard/soft ferrite-based $CoFe_2O_4/NiFe_2O_4$ nanocapsules

Chao Feng, Xianguo Liu, Siu Wing Or,[a] and S. L. Ho
Hong Kong Branch of National Rail Transit Electrification and Automation Engineering Technology Research Center, Hong Kong and Department of Electrical Engineering, The Hong Kong Polytechnic University, Hung Hom, Kowloon, Hong Kong

(Presented 3 November 2016; received 23 September 2016; accepted 6 October 2016; published online 20 December 2016)

Core/shell-structured, hard/soft spinel-ferrite-based $CoFe_2O_4/NiFe_2O_4$ (CFO/NFO) nanocapsules with an average diameter of 17 nm are synthesized by a facile two-step hydrothermal process using CFO cores of ~15 nm diameter as the hard magnetic phase and NFO shells of ~1 nm thickness as the soft magnetic phase. The single-phase-like hysteresis loop with a high remnant-to-saturation magnetization ratio of 0.7, together with a small grain size of ~16 nm, confirms the existence of exchange-coupling interaction between the CFO cores and the NFO shells. The effect of hard/soft exchange coupling on the microwave absorption properties is studied. Comparing to CFO and NFO nanoparticles, the finite-size NFO shells and the core/shell structure enable a significant reduction in electric resistivity and an enhancement in dipole and interfacial polarizations in the CFO/NFO nanocapsules, resulting in an obvious increase in dielectric permittivity and loss in the whole S–Ku bands of microwaves of 2–18 GHz, respectively. The exchange-coupling interaction empowers a more favorable response of magnetic moment to microwaves, leading to enhanced exchange resonances in magnetic permeability and loss above 10 GHz. As a result, strong absorption, as characterized by a large reflection loss (*RL*) of -20.1 dB at 9.7 GHz for an absorber thickness of 4.5 mm as well as a broad effective absorption bandwidth (for *RL*<-10 dB) of 8.4 GHz (7.8–16.2 GHz) at an absorber thickness range of 3.0–4.5 mm, is obtained. [http://dx.doi.org/10.1063/1.4972805]

I. INTRODUCTION

Microwave absorbers operating in the gigahertz microwave range have become increasingly important to improve electromagnetic (EM) compatibility of electronic devices and systems as well as to minimize EM radiation and interference pollutions in our society.[1–3] Spinel-structured magnetic ferrites are considered as high-potential candidates for microwave absorbers because of their good dielectric and magnetic properties, high environmental stability, ease of preparation, and low cost.[4] In the spinel-structured ferrite family, $CoFe_2O_4$ (CFO) is a representative hard magnetic material with large magnetic moment and high anisotropy field, while $NiFe_2O_4$ (NFO) is a typical soft magnetic material with high saturation magnetization and static permeability.[5] However, pure CFO and NFO only show general microwave absorption properties because of the reduction in imaginary permeability with increasing frequency towards a few gigahertz in accordance with the Snoek limit.[4]

Exchange-coupled hard/soft bi-magnetic materials have received a special attention in recent years because the exchange-coupling interaction between the hard and soft magnetic phases will bring about additional flexibility and opportunity to tailor the overall properties of the materials.[4] Specifically, when both phases are sufficiently exchange-coupled with each other, the large magnetic moment

[a]Author to whom correspondence should be addressed: electronic mail: eeswor@polyu.edu.hk

and high anisotropy field in the hard magnetic phase and the high saturation magnetization and static permeability in the soft magnetic phase will be utilized to induce a cooperative effect and hence an improved microwave absorption ability.[6] Exchange coupling interaction and enhanced microwave absorption properties have ever been reported in nanocomposite $BaFe_{12}O_{19}/Ni_{0.5}Zn_{0.5}Fe_2O_4$-aligned microfibers.[5]

Core/shell-structured nanocapsules, typically comprising a magnetic nanoparticle core coated by a relatively thin dielectric shell of a few nanometer, have attracted considerable attention in recent years owing to their high potential to exhibit strong absorption, broad absorption bandwidth, small thickness, and low density in the desired microwave frequency range.[1,2,7] Various works have been carried out to study the effect of conducting, insulating, and semiconducting dielectric shells on the microwave absorption properties in order to reveal their underlying absorption mechanisms for an improved EM match.[1,5,7] Due to the similar crystal structure and atom size of CFO and NFO, it is impressive to synthesize core/shell-structured, hard/soft spinel-ferrite-based CFO/NFO nanocapsules and investigate the effect of exchange-coupling interaction on their microwave absorption properties. In this work, we report the use of a simple two-step hydrothermal process to synthesize such an interesting type of nanocapsules as well as the study of their phase, morphology, interface microstructure, composition, exchange-coupling interaction, and microwave absorption properties. The results are discussed and compared with their CFO and CFO nanoparticle counterparts, if any. Emphases are put on the investigation of exchange-coupling interaction in the CFO/NFO nanocapsules and its effect on the microwave absorption properties.

II. EXPERIMENTS

A facile two-step hydrothermal process was used to synthesize core/shell-structured CFO/NFO nanocapsules.[8] All of the reactants, including iron (III) nitrate nonahydrate ($Fe(NO_3)_3{\cdot}9H_2O$), cobalt (II) nitrate hexahydrate ($Co(NO_3)_2{\cdot}6H_2O$), nickel (II) nitrate hexahydrate ($Ni(NO_3)_2{\cdot}6H_2O$), sodium hydroxide (NaOH), and sodium citrate ($Na_3C_6H_5O_7$), were of analytical grade and without further purification. First, CFO nanoparticles were synthesized as the core. In a typical reaction, $Co(NO_3)_2{\cdot}6H_2O$ of 1.0 g and $Fe(NO_3)_3{\cdot}9H_2O$ of 1.4 g were dissolved in distilled water of 60 ml, and NaOH was added into the solution to modify the PH value to 12. After a continuous stirring for 1 h, the solution was transferred into a stainless steel autoclave of 100 ml with Teflon line and heated at 180 °C for 15 h. The CFO product was washed several times by distilled water and alcohol and then dried at 60 °C for 6 h. Second, the as-synthesized CFO product was coated with a layer of NFO shell to form CFO/NFO nanocapsules. In a typical reaction, the CFO product was dispersed in a solution having $Na_3C_6H_5O_7$ of 2 g dissolved in distilled water of 50 ml. The mixture was stirred for 40 min, and the modified CFO product was collected by magnetic separation. $Ni(NO_3)_2{\cdot}6H_2O$ of 1.0 g and $Fe(NO_3)_3{\cdot}9H_2O$ of 1.4 g were dissolved in distilled water of 60 ml, and the modified CFO product was re-dispersed in the solution. The PH value of the mixture was adjusted to 12 by adding NaOH. After a continuous stirring for 1 h, the mixture was transferred into the autoclave and heated at 180 °C for 15 h. The CFO/NFO product was washed several times by distilled water and alcohol before being dried at 60 °C for 6 h.

The phase analysis of the CFO, NFO, and CFO/NFO products was performed using an X-ray diffractometer (XRD, Bruker D8 Advance) with monochromatic Cu-$K\alpha$ radiation (λ=1.54 Å). Their morphology and interface nanostructure were evaluated using a transmission electron microscope (TEM, JEM 2100F) with an emission voltage of 200 kV. An energy dispersive spectrometer (EDS) integrated with the TEM was employed to analyze the compositions of the products. The magnetic hysteresis loop was measured by a physical property measurement system (Quantum Design PPMS-9T) under an applied magnetic field range of ±3 T. CFO/NFO nanocapsules of 30 wt.% were mixed with microwave-transparent paraffin to form paraffin-bonded CFO/NFO nanocapsule composites of toroidal shape with 7 mm outer diameter and 3 mm inner diameter. CFO and NFO nanoparticles were also fabricated into paraffin-bonded CFO and NFO nanoparticle composites for comparison and further discussion. The complex relative permittivity ($\varepsilon_r = \varepsilon_r' - j\varepsilon_r''$) and permeability ($\mu_r = \mu_r' - j\mu_r''$) of the composites were measured by a transmission/reflection coaxial line method in the 2–18 GHz microwave range using a vector network analyzer (Agilent N5244A). The frequency (f)

and thickness (d) dependence of reflection loss (RL) was calculated using[6,7]

$$RL = 20\log|(Z_{in} - Z_0)/(Z_{in} + Z_0)| \quad (1)$$

where $Z_{in} = Z_0(\mu_r/\varepsilon_r)^{1/2}\tanh\left[j(2\pi fd/c)(\mu_r\varepsilon_r)^{1/2}\right]$ is the input impedance of composite, Z_0~377 Ω is the characteristic impedance of air, $c = 3\times10^8$ m/s is the velocity of light, and d is the thickness of composite.

III. RESULTS AND DISCUSSION

Figure 1 shows the XRD patterns of typical CFO, NFO, and CFO/NFO products. For the CFO and NFO products, the diffraction peaks match well with face-centered cubic CFO (JCPDS card No. 01-1121) and NFO (JCPDS card No. 54-0964), respectively.[9,10] The XRD pattern of the CFO/NFO product is very similar to the CFO and NFO products even though there are some differences in both intensity and full width at half maximum (FWHM). The observation suggests a constitution of CFO and NFO in the CFO/NFO product. The intensity and FWHM of the CFO/NFO peaks are comparatively larger and narrower, respectively, indicating the existence of a higher degree of crystallization and a larger particle size in the CFO/NFO product.

Figures 2(a) and 2(b) illustrate the TEM image and EDS pattern of a typical CFO product, while Figs. 2(c) and 2(d) display those of a typical CFO/NFO product. From the TEM images, both CFO and CFO/NFO products are in spherical shape, and their average sizes are ~14 and ~16 nm, respectively. From the EDS patterns, the CFO nanoparticles are composed of Co, Fe, and O elements, while the CFO/NFO nanoparticles are made up of Co, Fe, O, and Ni elements. The detection of an additional Ni element in the CFO/NFO nanoparticles reflects the formation of a NFO layer besides the CFO nanoparticles. Figure 2(e) shows the TEM image of the CFO/NFO product in Fig. 2(c) with a higher magnification. A core/shell structure is apparently seen. Figure 2(f) gives the HRTEM of the CFO/NFO product in Fig. 2(e). A spherical nanoparticle of ~15 nm diameter is coated with a shell of ~1 nm thickness (0.89 nm as marked in Fig. 2(f)). The lattice plane spacing of the core is found to be 0.29 nm, which agrees well with the d-spacing of (220) planes of CFO. The good agreement confirms the successful synthesis of the core/shell-structured CFO/NFO nanocapsules with an average diameter of 17 nm using the CFO nanoparticles of ~15 nm diameter as the core and the NFO layers of ~1 nm thickness as the shell.

Figure 3 plots the measured magnetic hysteresis (M–H) loops of the CFO nanoparticles, NFO nanoparticles, CFO/NFO nanocapsules, and mixture of CFO and NFO nanoparticles. The coercive field of the CFO nanoparticles (=6070 Oe) is much larger than that of the NFO nanoparticles (=320 Oe) owing to the exhibition of the intrinsic magnetic properties of the hard and soft magnetic materials, respectively. The hysteresis loop of the CFO/NFO nanocapsules is very strong and smooth in that its coercive field (=6400 Oe) is even larger than that of the CFO nanoparticles (=6070 Oe). This is due to the presence of a single-phase-like magnetic material behavior in the CFO/NFO nanocapsules as

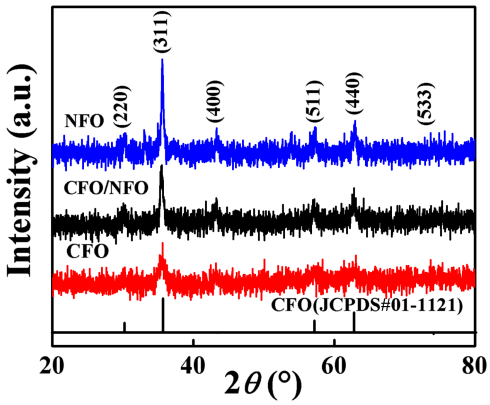

FIG. 1. XRD patterns of typical CFO, NFO, and CFO/NFO products.

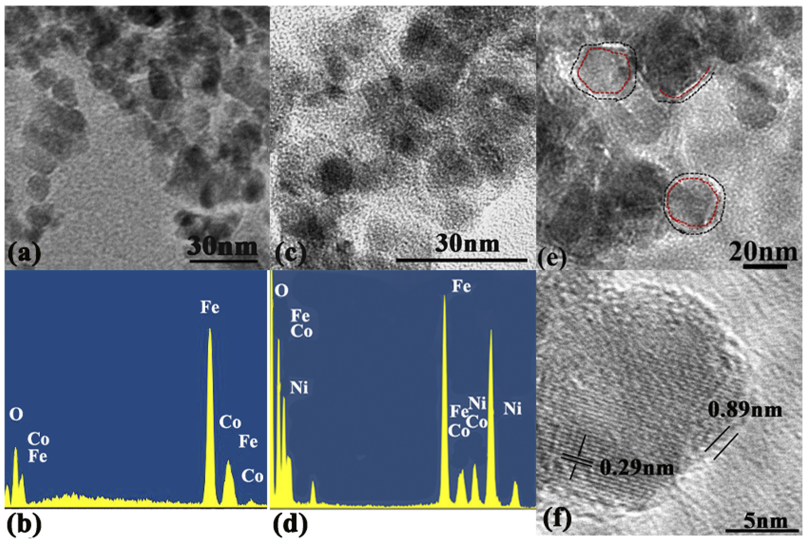

FIG. 2. (a) TEM image and (b) EDS pattern of a typical CFO product. (c) TEM and (d) EDS pattern of a typical CFO/NFO product. (e) TEM image of CFO/NFO product in (c). (f) HRTEM of CFO/NFO product in (e).

a result of the exchange-coupling interaction between the CFO cores and the NFO shells. In other words, the hard CFO cores and the soft NFO shells are properly exchange-coupled together, and the magnetization of both material phases reverses cooperatively. In fact, the grain size of the CFO/NFO nanocapsules is ~16 nm (Fig. 2(f)), which is favorable for exchange coupling interaction.[6] Moreover, the ratio of remnant magnetization to saturation magnetization (M_r/M_s) of the CFO/NFO nanocapsules is 0.7 (M_r=29.7 emu/g and M_s=42.7 emu/g in Fig. 3). This value is well above the threshold ratio of 0.5 in accordance with the Stoner-Wohlfarth theory,[11] further supporting the existence of an exchange-coupling interaction in the CFO/NFO nanocapsules. By contrast, the mixture of CFO and NFO nanoparticles demonstrates a typical bee-waist-type hysteresis loop, elucidating the high independence of the two phases and the inexistence of any exchange-coupling interaction.[11]

Figures 4(a) and 4(b) show the measured f dependence of ε_r' and ε_r'' of the CFO, NFO, and CFO/NFO composites, respectively. The ε_r' and ε_r'' responses of the CFO and NFO composites are generally weak and demonstrate very similar quantitative variations with each other throughout the whole f range of measurement because of their very similar nanoparticle size and electric properties. By comparison, ε_r' and ε_r'' of the CFO/NFO composite are significantly stronger and exhibit obvious decreasing trends from 5.3 to 3.4 and from 3.2 to 1.0, respectively, in the 2–18 GHz microwave range. According to the free electron theory,[12] $\varepsilon_r'' \approx 1/2\pi\rho f$, where ρ is the electric resistivity. A large ε_r''

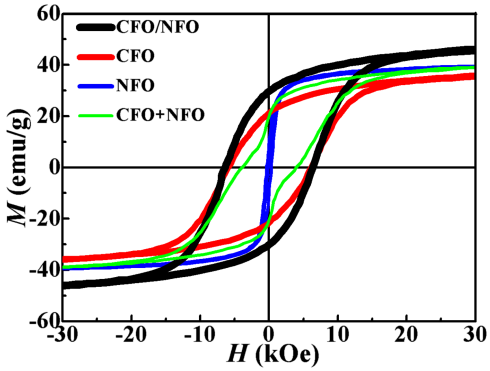

FIG. 3. Measured magnetic hysteresis (M–H) loops of CFO nanoparticles, NFO nanoparticles, CFO/NFO nanocapsules, and mixture of CFO and NFO nanoparticles.

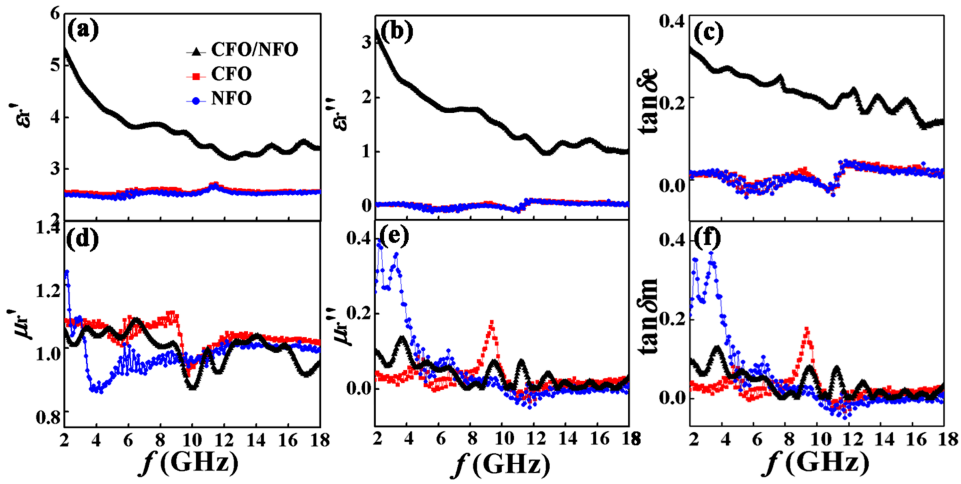

FIG. 4. Measured f dependence of (a) ε_r', (b) ε_r'', (c) $\tan\delta_e$, (d) μ_r', (e) μ_r'', and (f) $\tan\delta_m$ of CFO, NFO, and CFO/NFO composites.

implies a low electric resistivity or a high electric conductivity. Zabotto *et al.* reported that the electric resistivity of NFO nanoparticles decreases dramatically with decreasing size.[13] In our case, the NFO shells are as thin as ~1 nm thickness, which can significantly reduce the overall resistivity of the CFO/NFO nanocapsules and hence that of their composites. Thus, the significant increase in ε_r'' in our case indicates a significant decrease in resistivity and a corresponding increase in dielectric loss. In general, the dielectric loss includes electronic, ionic, dipole, and interfacial polarizations. Since electronic and ionic polarizations are only effective in the megahertz range, the main contributors for the dielectric loss are dipole and interfacial polarizations. The dielectric resonance peaks as seen at 8.6, 11.6, 13.8, and 15.6 GHz may be attributed to the dipole polarization of each constituent component in the CFO/NFO composite (i.e., CFO, NFO, and paraffin) and the interfacial polarization between the CFO cores and NFO shells.[14]

Figures 4(d) and 4(e) show the measured f dependence of μ_r' and μ_r'' of the CFO, NFO, and CFO/NFO composites, respectively. The μ_r' and μ_r'' responses of all composites exhibit decreasing trends with increasing f with multiple magnetic resonances. The appearance of the resonance peaks at 8–10 and 2–6 GHz in the CFO and NFO composites further proves the hard and soft magnetic material natures of the CFO and NFO nanoparticles, respectively. For the CFO/NFO composite, the resonance peaks are detected above 10 GHz because magnetic moment can easily respond to applied microwaves under the exchange-coupling interaction between the CFO cores and the NFO shells.[4,5] It is seen that μ_r'' of all composites gives negative values at some f because of the cancellation of external magnetic fields by additional magnetic fields induced by eddy currents.[15,16]

Figures 4(c) and 4(f) show the calculated f dependence of dielectric loss tangent ($\tan\delta_e = \varepsilon_r''/\varepsilon_r'$) and magnetic loss tangent ($\tan\delta_m = \mu_r''/\mu_r'$) of the CFO, NFO, and CFO/NFO composites, respectively. $\tan\delta_e$ and $\tan\delta_m$ of all composites exhibit similar quantitative trends with their respective ε_r'' and μ_r'' in Figs. 4(b) and 4(e), respectively. This similarity suggests the dominant effect of ε_r'' and μ_r'' on $\tan\delta_e$ and $\tan\delta_m$, respectively. On the other hands, $\tan\delta_e$ and $\tan\delta_m$ values of the CFO/NFO composite are obviously larger than those of the CFO and NFO composites due to the interfacial polarization and the exchange-coupling interaction, respectively. These loss tangents are the main loss contributors to the absorption ability of the CFO/NFO nanocapsules and their composites. The higher the loss tangent value, the larger the loss is.

Figure 5(a), 5(b), and 5(c) show the calculated f dependence of RL at different d for the CFO, NFO, and CFO/NFO composites, respectively. RL as strong as -20.1 dB is obtained at 9.7 GHz for d=4.5 mm. The optimized RL of -3.9 dB at 9.4 GHz and d=4.5 mm is significantly weaker and narrow in the CFO composite. The RL response in the NFO composite is even poor with no useable RL peak. Moreover, the effective absorption bandwidth for RL<-10 dB, corresponding to 90% absorption, is as wide as 8.4 GHz (i.e., 7.8–16.2 GHz) in the CFO/NFO composite in that it essentially covers the

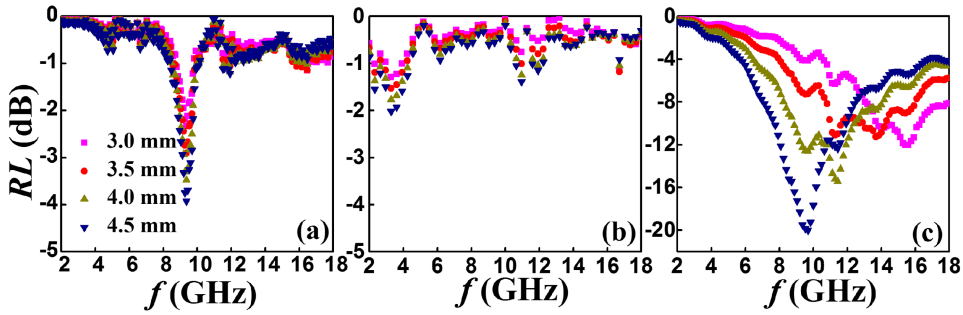

FIG. 5. Calculated f dependence of RL at different d for (a) CFO, (b) NFO, and (C) CFO/NFO composites.

full X (8–12 GHz) band and the major portion of Ku (12–18 GHz) band of microwaves for the d range of 3.0–4.5 mm. In addition, the shift in RL peak to the lower frequency side with increasing f can be explained by the quarter-wavelength theory.[16]

IV. CONCLUSION

We have synthesized core/shell-structured, hard/soft spinel-ferrite-based CFO/NFO nanocapsules with CFO cores of ~15 nm diameter and NFO shells of ~1 nm thickness by a simple two-step hydrothermal process as well as studied their phase, morphology, interface microstructure, composition, exchange-coupling interaction, and microwave absorption properties. We have discussed and compared the results with their CFO and CFO nanoparticle counterparts. The single-phase-like hysteresis loop with a high M_r/M_s of 0.7 and small grain size of ~16 nm have proven the existence of exchange-coupling interaction between the CFO cores and the NFO shells. The finite-size NFO shells and the core/shell structure have reduced electric resistivity and enhanced dipole and interfacial polarizations so as to increase dielectric permittivity and loss in the whole S–Ku microwave bands of 2–18 GHz, respectively. The established exchange-coupling interaction has promoted magnetic moment response to microwaves in order to enhance exchange resonances in magnetic permeability and loss above 10 GHz. The improved dielectric and magnetic losses have resulted in a large RL of -20.1 dB at 9.7 GHz for d=4.5 mm and a broad effective absorption bandwidth (for RL<-10 dB) of 8.4 GHz (7.8–16.2 GHz) at the d range of 3.0–4.5 mm.

ACKNOWLEDGMENTS

This work was supported by the Innovation and Technology Commission of the HKSAR Government to the Hong Kong Branch of National Rail Transit Electrification and Automation Engineering Technology Research Center under Grant No. 1-BBYF and The Hong Kong Polytechnic University under Grant No. G-YBLL.

[1] N. D. Wu, X. G. Liu, C. Y. Zhao, C. Y. Cui, and J. J. Guo, J. Alloys Compd. **685**, 50 (2016).
[2] X. Wang, Q. F. Li, Z. J. Su, W. Gong, R. Z. Gong, Y. J. Chen, and V. G. Harris, J. Alloys Compd. **643**, 111 (2016).
[3] M. F. Li, J. J. Guo, and B. S. Xu, Appl. Phys. Lett. **102**, 121904 (2013).
[4] T. Maeda, S. Sugimoto, T. Kagotani, N. Tezuka, and K. Inomata, J. Magn. Magn. Mater. **281**, 195 (2004).
[5] X. Q. Shen, F. Z. Song, J. Xiang, M. Q. Liu, Y. W. Zhu, and Y. D. Wang, J. Am. Ceram. Soc. **95**, 3863 (2012).
[6] N. D. Wu, X. G. Liu, and S. W. Or, AIP Adv. **6**, 056206 (2006).
[7] X. G. Liu, S. W. Or, C. G. Jin, and C. Feng, Carbon **60**, 215 (2013).
[8] W. X. Li, L. C. Wang, G. M. Li, and Y. Xu, J. Alloy. Compd. **633**, 11 (2015).
[9] F. Ren, G. M. Zhu, P. G. Ren, K. Wang, X. P. Cui, and X. G. Yan, Appl. Surf. Sci. **351**, 40 (2015).
[10] H. T. Zhao, X. D. Sun, C. H. Mao, and J. Du, Physica B **404**, 69 (2009).
[11] Q. Z. Zeng, D. M. Jiang, and S. B. Yang, RSC Adv. **6**, 46143 (2016).
[12] X. G. Liu, N. D. Wu, C. Y. Cui, N. N. Bi, and Y. P. Sun, RSC Adv. **5**, 24016 (2015).
[13] F. L. Zabotto, A. J. Gualdi, J. A. Eiras, A. J. Aparecido de Oliveira, and D. Garcia, Mater. Res. **15**, 428 (2012).
[14] Z. H. Wang, Z. Han, D. Y. Geng, and Z. D. Zhang, Chem. Phys. Lett. **489**, 187 (2010).
[15] J. N. Li, X. Wang, K. Song, Q. F. Li, R. Z. Gong, and Z. J. Su, IEEE Trans. Magn. **51**, 1 (2015).
[16] N. D. Wu, X. G. Liu, C. Y. Zhao, C. Y. Cui, and J. J. Guo, J. Alloys Compd. **685**, 50 (2016).